remote sensing

MDPI

Article

Spatiotemporal Variation of Water Use Efficiency and Its Responses to Climate Change in the Yellow River Basin from 1982 to 2018

Jie Li [1,2,†], Fen Qin [3,4,5,†], Yingping Wang [6], Xiuyan Zhao [7], Mengxiao Yu [1,2], Songjia Chen [1,2], Jun Jiang [1,2], Linhua Wang [1,2] and Junhua Yan [1,2,*]

[1] National Ecological Science Data Center Guangdong Branch, South China Botanical Garden, Chinese Academy of Sciences, 723 Xingke Road, Guangzhou 510650, China; lhwang@scbg.ac.cn (L.W.)
[2] South China National Botanical Garden, Guangzhou 510650, China
[3] College of Geography and Environmental Science, Henan University, Kaifeng 475004, China
[4] Key Laboratory of Geospatial Technology for the Middle and Lower Yellow River Regions, Ministry of Education, Henan University, Kaifeng 475004, China
[5] Henan Industrial Technology Academy of Spatio-Temporal Big Data, Henan University, Kaifeng 475004, China
[6] CSIRO Oceans and Atmosphere, Aspendale, VIC 3195, Australia; yingping.wang@csiro.au
[7] School of Geography and Planning, Sun Yat-sen University, Guangzhou 510275, China
* Correspondence: jhyan@scib.ac.cn
† These authors contributed equally to this work.

Abstract: The ecosystem water use efficiency (WUE) plays a critical role in many aspects of the global carbon cycle, water management, and ecological services. However, the response mechanisms and driving processes of WUE need to be further studied. This research was conducted based on Gross Primary Productivity (GPP), Evapotranspiration (ET), meteorological station data, and land use/cover data, and the methods of Ensemble Empirical Mode Decomposition (EEMD), trend variation analysis, the Mann–Kendall Significant Test (M-K test), and Partial Correlation Analysis (PCA) methods. Our study revealed the spatio-temporal trend of WUE and its influencing mechanism in the Yellow River Basin (YRB) and compared the differences in WUE change before and after the implementation of the Returned Farmland to Forestry and Grassland Project in 2000. The results show that (1) the WUE of the YRB showed a significant increase trend at a rate of 0.56×10^{-2} gC·kg^{-1}·H_2O·a^{-1} ($p < 0.05$) from 1982 to 2018. The area showing a significant increase in WUE (47.07%, Slope > 0, $p < 0.05$) was higher than the area with a significant decrease (14.64%, Slope < 0, $p < 0.05$). The region of significant increase in WUE in 2000–2018 (45.35%, Slope > 0, $p < 0.05$) was higher than that of 1982–2000 (8.23%, Slope > 0, $p < 0.05$), which was 37.12% higher in comparison. (2) Forest WUE (1.267 gC·kg^{-1}·H_2O) > Cropland WUE (0.972 gC·kg^{-1}·H_2O) > Grassland WUE (0.805 gC·kg^{-1}·H_2O) under different land cover types. Forest ecosystem WUE has the highest rate of increase (0.79×10^{-2} gC·kg^{-1}·H_2O·a^{-1}) from 2000 to 2018. Forest ecosystem WUE increased by 0.082 gC·kg^{-1}·H_2O after 2000. (3) precipitation (37.98%, R > 0, $p < 0.05$) and SM (10.30%, R > 0, $p < 0.05$) are the main climatic factors affecting WUE in the YRB. A total of 70.39% of the WUE exhibited an increasing trend, which is mainly attributed to the simultaneous increase in GPP and ET, and the rate of increasing GPP is higher than the rate of increasing ET. This study could provide a scientific reference for policy decision-making on the terrestrial carbon cycle and biodiversity conservation.

Keywords: water use efficiency; GPP; ET; spatiotemporal analysis; partial correlation analysis; Yellow River Basin

check for updates

Academic Editor: Jean-Christophe Calvet

Received: 14 November 2024
Revised: 14 January 2025
Accepted: 15 January 2025
Published: 17 January 2025

Citation: Li, J.; Qin, F.; Wang, Y.; Zhao, X.; Yu, M.; Chen, S.; Jiang, J.; Wang, L.; Yan, J. Spatiotemporal Variation of Water Use Efficiency and Its Responses to Climate Change in the Yellow River Basin from 1982 to 2018. *Remote Sens.* **2025**, *17*, 316. https://doi.org/10.3390/rs17020316

Copyright: © 2025 by the authors. Licensee MDPI, Basel, Switzerland. This article is an open access article distributed under the terms and conditions of the Creative Commons Attribution (CC BY) license (https://creativecommons.org/licenses/by/4.0/).

1. Introduction

The water use efficiency (WUE) plays a crucial role in energy transfer and water movement, serving as a vital link among the interactions of the geosphere, biosphere, and atmosphere [1–3]. WUE serves as a metric for assessing carbon-water interactions within ecosystem vegetation; using Gross Primary Productivity (GPP) and Evapotranspiration (ET) data to study WUE is a common method in the fields of ecology and geography [4,5]. In natural ecosystems, WUE significantly affects plant distribution, ecosystem structure, and the dynamics of both carbon and water cycles [6–8].

With the intensification of global climate change, precipitation patterns are becoming increasingly erratic, and the frequency of droughts is increasing [9,10]. Enhancing WUE in crops and ecosystems is essential for optimizing water resource allocation and utilization, thereby promoting sustainable management in the face of dwindling water resources [6,7,11]. WUE can effectively reflect the variations and interactions of carbon and water cycles [12,13]. Consequently, investigating the spatiotemporal variations in ecosystem WUE and its underlying factors will advance our understanding of the carbon cycle. This research will also offer valuable insights for the optimal management of regional water resources and ecosystem services [14–16].

In recent years, the escalating effects of climate change have become increasingly apparent [17–19]. Research on the WUE in terrestrial ecosystems is providing new insights for mitigating greenhouse gas emissions and addressing the challenges associated with climate change [20–24]. Tesfaye et al. [25] found that WUE was higher in semi-arid regions compared to humid areas, indicating that temperature and precipitation significantly influence changes in ET and WUE. Xue et al. [26] showed that both GPP and WUE exhibited significant increasing trends, with rates of 10.53 gCm^{-2} yr^{-1} and 0.01 $gC{\cdot}kg^{-1}$ H_2O yr^{-1}, respectively. Furthermore, GPP played a crucial role in WUE changes, accounting for over 79.51% of the total area. An et al. [4] observed a declining trend in vegetation WUE in Xinjiang from 2000 to 2014, with temperature having a significant impact on WUE (87.7%). Chang et al. [2] identified the Leaf Area Index (LAI) as the primary factor influencing variations in grassland WUE on the Loess Plateau. Zhang et al. [16] observed that the rate of increase in vegetation WUE was highest in the water-scarce regions of the Loess Plateau, with grassland WUE and its growth rate surpassing those of other ecosystem types. Climate change threatens ecosystems and the species; the WUE research is more necessary, as it offers a scientific foundation for the advanced development of ecological systems and the creation of strategies for water resource management.

The Yellow River Basin (YRB) extends throughout China's dry and semi-arid regions, where the ecological environment is fragile and sensitive to climate change [27,28]. For a long time, water resource issues have been a critical factor hindering the ecologically sustainable development of the YRB [29]. WUE is a key indicator of how terrestrial ecosystems respond to both climatic and non-climatic factors [30,31]. However, the trends in WUE within the YRB and its responses to major climatic factors remain unclear. Moreover, there is a shortage of research on the differences in water use efficiency variations before and after the Returned Farmland to Forestry and Grassland Project in 2000 [26,32,33]. Therefore, investigating the characteristic changes in WUE and its primary influencing factors across different time periods has become an urgent necessity for ecological protection and water resource management. This research offers valuable recommendations for promoting high-quality development and biodiversity conservation.

2. Materials and Methods

2.1. Study Area

The YRB is located in the north of China (Figure 1) and is the second largest river in China [26,30]. It is located between 95°53′–119°05′E and 32°10′–41°50′N, about 1100 km wide from north to south and 1900 km long from east to west. It stretches across nine provinces in China [34,35]. The topography of the Yellow River Basin is characterized by high west and low east, with large differences in elevation, forming a three-step terrain from west to east, gradually from high to low [9]. There are significant climatic differences between different regions in the YRB, where the ecological environment is fragile and sensitive to climate change.

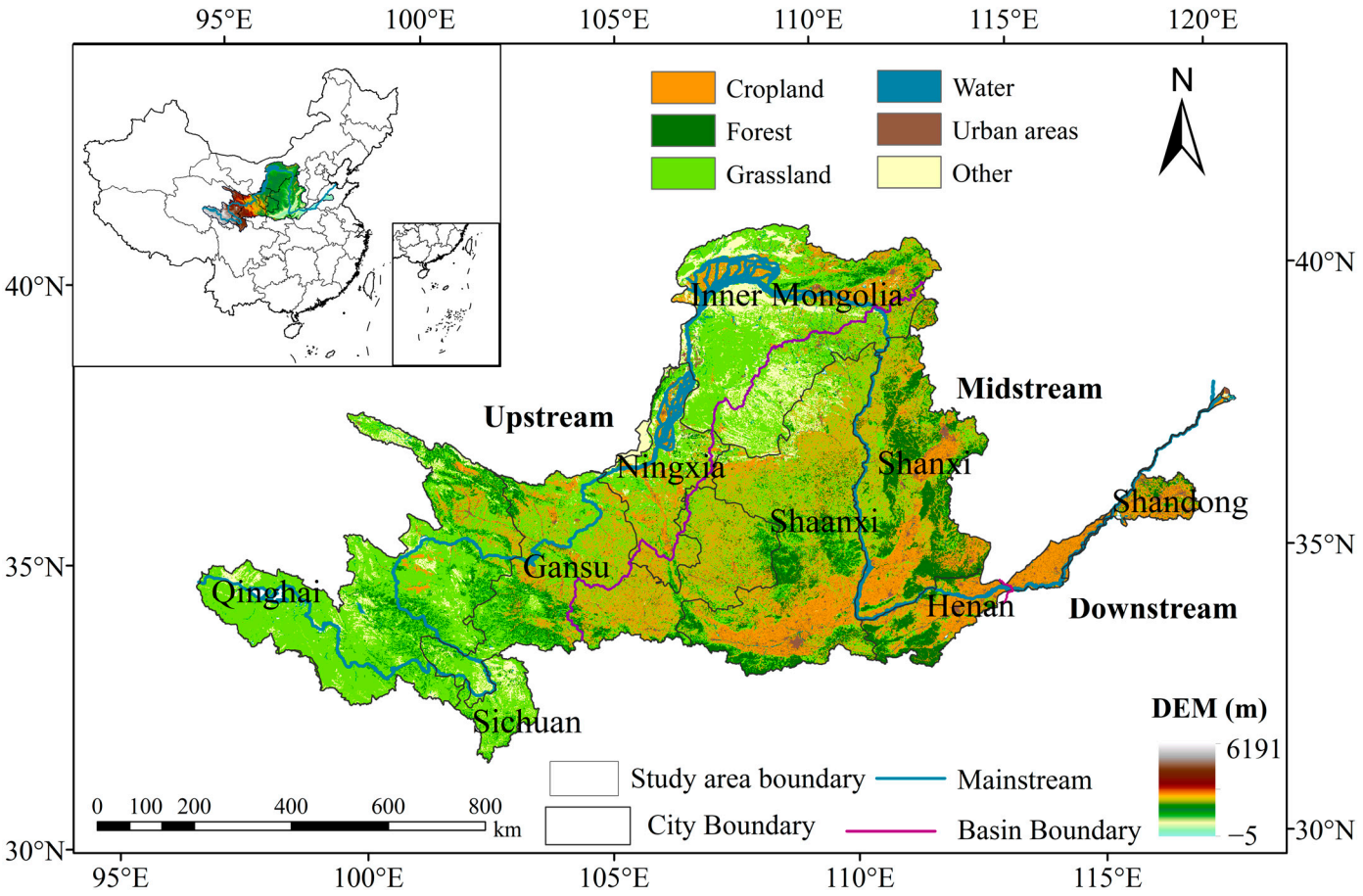

Figure 1. Study area, vegetation type, basin boundary, and elevation.

2.2. Datasets

2.2.1. GPP Dataset

The Global Monthly Vegetation GPP product dataset from 1982 to 2018, which was generated based on Near-infrared Reflectance Vegetation index (NIRv) inversion (https://www.geodata.cn/, accessed on 10 June 2022). This dataset was characterized by medium-to high resolution, with a spatiotemporal resolution of 5 km and monthly [30,36]. This dataset formats typically include spatial data formats, such as GeoTIFF, HDF5, etc. GPP dataset can provide strong scientific support for global ecosystem evolutionary patterns, ecological monitoring, resource development, and sustainable socio-economic development [36].

2.2.2. Evapotranspiration and Soil Moisture Datasets

The Evapotranspiration (ET) data were obtained from the Global land surface satellite (GLASS) products actual evapotranspiration dataset [4,24], publicly accessible at the University of Maryland GLASS Data Center (http://www.glass.umd.edu/, accessed on 19 July 2022). The GLASS ET product was characterized by a long time series (1981–2018), spatiotemporal resolution was 5 km and 8 days (http://www.glass.umd.edu/, accessed on 19 July 2022), giving it an advantage over existing ET products [4,28]. The soil moisture (SM) information was obtained from the climate reanalysis database [37,38], and is open for freely downloadable access to a large amount of climate data (https://www.ecmwf.int/, accessed on 19 July 2023).

2.2.3. Meteorology Data

The meteorology data sourced from the China Meteorological Data Center are an important component of meteorological monitoring and analysis (http://data.cma.cn/, accessed on 17 June 2022). This study used the interpolation method to construct monthly temperature and precipitation raster data [34,39]. These data are important for predicting weather changes, guiding agricultural production, and urban planning.

2.2.4. Land Use/Cover Data

The Land Use/Cover data provided by the Resource and Environmental Sciences Data Center (RESDC) (https://www.resdc.cn/, accessed on 10 May 2022). The dataset has a spatiotemporal resolution of 1 km and each 5 years. The dataset was constructed by visual interpretation using Landsat remote sensing image data as the main source of information [40,41]. The study mainly selected remote sensing information sources for land use/land cover classification (LUCC) by using visible and near-infrared wavelength [42]. In order to maintain consistency in the spatial resolution of the research subjects, we have employed nearest neighbor interpolation methods to standardize the spatial resolution.

2.3. Methods

2.3.1. Ensemble Empirical Mode Decomposition (EEMD)

EEMD can effectively handle nonlinear and non-stationary signals, and it is widely used in various fields [43]. In the domain of remote sensing and earth sciences, EEMD is more helpful in extracting useful information and trends to better understand the dynamics of the earth system [44,45]. The mathematics of EEMD is as follows:

Step 1: The white noise sequence $N(t)$ is added to the original signal $e(t)$, generating a new time series $E(t)$. The formula is:

$$E(t) = e(t) + N(t) \tag{1}$$

Step 2: N repetitions repeated the first and second steps and added $N(t)$.

$$E(t) = \sum_{i=1}^{n} IMF_i(t) + R_n(t) \tag{2}$$

Step 3: After the Step 2 several Intrinsic Mode Function (IMFs) can be obtained, and then several IMFs are averaged to obtain a new IMF, which is then represented as $IMF_{nj}(t)$. The formula is:

$$IMF_n(t) = \frac{1}{Z}\sum_{j=1}^{n} IMF_{nj}(t) \tag{3}$$

$$R_m(t) = \frac{1}{Z}\sum_{j=1}^{n} R_{mj} \tag{4}$$

where $IMF_n(t)$ is a single IMF component and $R_m(t)$ is the trend item. Therefore, E (t) can be decomposed as:

$$E(t) = \sum_{n=1}^{m} IMF_n(t) + R_m(t) \quad (5)$$

2.3.2. Mann–Kendall Significant Test (M-K Test)

The M-K test method can indeed examine the trend of a time series and also detect whether a mutation has occurred [46,47]. Because the method does not require the sample information to obey a certain distribution, with the advantage of less influence of outliers [48]. Therefore, it has become an effective method to test the trend of time series elements. The formula is as follows:

$$Z_c = \begin{cases} \frac{W-1}{\sqrt{var(W)}} & W > 0 \\ 0 & W = 0 \\ \frac{W+1}{\sqrt{var}} & W < 0 \end{cases} \quad (6)$$

$$S = \sum_{k=1}^{n-1} \sum_{j=k+1}^{n} sign(W_k - W_j) \quad (7)$$

$$var(S) = \frac{n(n-1)(2n+5) - \sum_{k=1}^{n} t_k(t_k-1)\,(2t_k+5)}{18} \quad (8)$$

$$sign(W_k - W_i) = \begin{cases} 1 & W_k - W_j > 0 \\ 0 & W_k - W_j = 0 \\ -1 & W_k - W_j < 0 \end{cases} \quad (9)$$

where W_k and W_j denote the WUE in year k and year j, respectively. α represents the significance level, when $|Z_c| > Z_{1-\alpha/2}$, it means that the sequence changes significantly at the α level. In this research was mainly used for significance analysis of WUE.

2.3.3. Trend Variation Analysis

Trend variation analysis was used to calculate the rate of variation for geographic elements in the long time series [34,47], to characterize the average rate of change and the trend of the time series. The formula is:

$$Slope = \frac{n\sum_{n}^{i=1} X_i N_i - \sum_{n}^{i=1} X_i \sum_{n}^{i=1} N_i}{n\sum_{n}^{i=1} X_i{}^2 - \left(\sum_{n}^{i=1} X_i\right)^2} \quad (10)$$

where n represents the year; X_i and N_i are the values of WUE for monitoring year i, respectively; Slope is the regression slope.

2.3.4. Partial Correlation Analysis (PCA)

Since traditional methods of correlation analysis may not adequately take into account the interrelationships between multiple variables [49,50]. Therefore, when analyzing the driven factors of WUE change, we chose to use partial correlation analysis (PCA) to address the interactions between multiple factors. The calculation formula is as follows:

$$R_{ab,c} = \frac{R_{ab} - R_{ac}R_{bc}}{\sqrt{(1-R_c^2)\,(1-R_{bc}^2)}} \quad (11)$$

where $R_{ab,c}$ represent the partial correlation coefficient (PCC) between variable a and b when variable c is considered as a constant, R_{ab}, R_{ac}, R_{bc} represent the partial correlation coefficients of a, b, c with each other.

3. Results

3.1. Characterization of Spatiotemporal Variations

3.1.1. Temporal Trends

The time series analysis of WUE from 1982 to 2018 (Figure 2) revealed that both annual and growing season WUE exhibited an increasing trend in the YRB. Between 1982 and 2018, there were similar fluctuating characteristics observed in both the annual WUE and the growing season WUE. The annual WUE (0.56×10^{-2} gC·kg^{-1}·H$_2$O·a^{-1}, $R^2 = 0.5478$) and growing season WUE (0.44×10^{-2} gC·kg^{-1}·H$_2$O·a^{-1}, $R^2 = 0.5171$) exhibited a significant increasing trend. The annual WUE variation rate was 0.48×10^{-2} gC·kg^{-1}·H$_2$O·a^{-1} ($R^2 = 0.15$) and 0.41×10^{-2} gC·kg^{-1}·H$_2$O·a^{-1} ($R^2 = 0.1985$) in 1982–2000 and 2000–2018, respectively. The growing season WUE revealed a gradual increasing trend at the rate of 0.39×10^{-2} gC·kg^{-1}·H$_2$O·a^{-1} ($R^2 = 0.1479$) and 0.29×10^{-2} gC·kg^{-1}·H$_2$O·a^{-1} ($R^2 = 0.1465$) in 1982–2000 and 2000–2018, respectively. The average WUE of the YRB from 1982 to 2018 was 0.93 gC·kg^{-1}·H$_2$O, with the highest value of 1.10 gC·kg^{-1}·H$_2$O, which the highest value appeared in 2018, and the lowest value of 0.72 gC·kg^{-1}·H$_2$O, which the lowest value appeared in 1982. According to the time series trend of Figure 2, it was found that the ecosystem WUE of the YRB from 2000 to 2018 (Mean value: 0.99 gC·kg^{-1}·H$_2$O) is higher than that before 2000 (Mean value: 0.87 gC·kg^{-1}·H$_2$O).

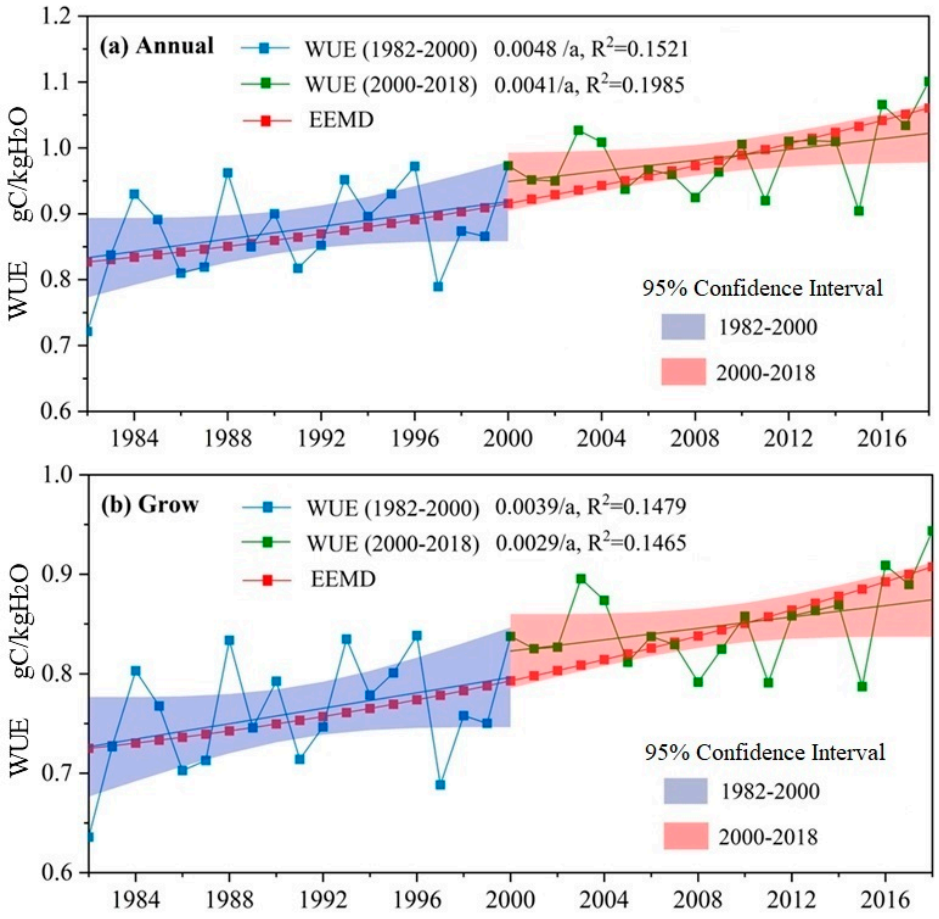

Figure 2. Temporal trends of WUE in 1982–2018. (**a**) Annual; (**b**) Grow.

Table 1 revealed the WUE of the upstream, midstream and downstream throughout the year, growing season and different seasons in the YRB. During 1982–2018 in the upstream of the YRB, the WUE was 1.08 gC·kg^{-1}·H$_2$O, 1.36 gC·kg^{-1}·H$_2$O, 1.93 gC·kg^{-1}·H$_2$O,

0.29 gC·kg^{-1}·H_2O in spring, summer, fall, and winter, respectively. Among them, the autumn has the highest WUE. The order of magnitude is: autumn > summer > spring > winter. The autumn WUE in the midstream and downstream of the YRB was higher than that in other seasons, which was 2.38 gC·kg^{-1}·H_2O and 2.42 gC·kg^{-1}·H_2O, respectively, and the downstream was higher than that in the midstream. Compared the WUE of the upstream, midstream and downstream at different seasonal scales, it was found that the WUE in autumn was significantly higher than that in spring, summer and winter at different geographic zones, and the WUE was the lowest in winter.

Table 1. Statistics on WUE in the YRB from 1982 to 2018. (Unit: gC·kg^{-1}·H_2O).

	Upstream			Midstream			Downstream		
	Mean	**Max**	**Min**	**Mean**	**Max**	**Min**	**Mean**	**Max**	**Min**
Annual	1.04	1.24	0.75	0.81	0.97	0.59	0.95	1.18	0.78
Grow	0.90	1.06	0.67	0.70	0.83	0.52	0.84	1.04	0.69
Spring	1.08	1.63	0.66	1.48	1.87	1.20	1.46	1.82	0.90
Summer	1.36	1.57	1.02	1.15	1.35	0.82	1.48	1.87	1.20
Autumn	1.93	2.38	1.38	2.38	2.84	1.99	2.42	2.91	2.04
Winter	0.29	0.58	0.03	0.15	0.32	0.02	0.41	0.84	0.11

3.1.2. Characteristics of Spatial Variation

Figure 3 depicted the regional variation features of WUE in different periods, the WUE showed a spatially heterogeneous distribution characterized by a gradually decreasing trend from the southwest to the northeast. The WUE during both 1982–2000 and 2000–2018 exhibited similar spatial distribution patterns, progressively decreasing from southwest to northeast during 1982–2018.

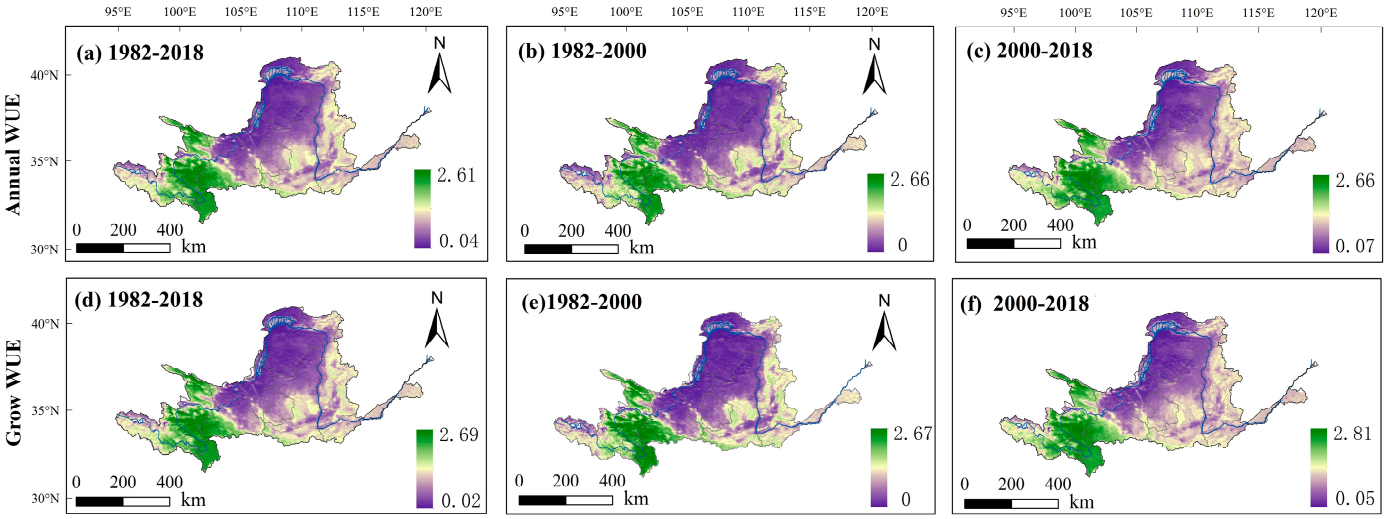

Figure 3. Spatial variation characteristics of WUE in the YRB. (**a**) Annual WUE in 1982–2018; (**b**) Annual WUE in 1982–2000; (**c**) Annual WUE in 2000–2018; (**d**) Grow WUE in 1982–2018; (**e**) Annual WUE in 1982–2000; (**f**) Annual WUE in 2000–2018.

The annual average WUE of the YRB from 1982 to 2018 was 0.93 gC·kg^{-1}·H_2O, and the distribution value range was between 0.04 gC·kg^{-1}·H_2O and 2.61 gC·kg^{-1}·H_2O. The regions with high values of annual average WUE (>1.60 gC·kg^{-1}·H_2O) are mainly located in Qinghai, northern Sichuan, southwestern Gansu, southern Shaanxi, eastern Shanxi and parts of Henan. The region of low values (<0.52 gC·kg^{-1}·H_2O) is predominantly found in the upstream and midstream areas of the YRB, mainly covering northwestern Qing-

hai, northeastern Gansu, Ningxia, northern Shaanxi, and much of Inner Mongolia. The WUE from 1982 to 2000 was 0.88 $gC \cdot kg^{-1} \cdot H_2O$, with a range of values between 0 and 2.66 $gC \cdot kg^{-1} \cdot H_2O$, while the average annual WUE from 2000 to 2018 was 0.99 $gC \cdot kg^{-1} \cdot H_2O$, with a range of values between 0.07 and 2.66 $gC \cdot kg^{-1} \cdot H_2O$, WUE was increased by 0.11 $gC \cdot kg^{-1} \cdot H_2O$ from 2000 to 2018 relative to 1982–2000. The WUE exhibited a pattern of progressive decrease in spatial distribution from the southwest to the northeast across the periods 1982–2000 and 2000–2018. The results indicated that there were differential characteristics in the WUE of the YRB before and after 2000, but there were similarities in the characteristics of its spatial distribution.

3.1.3. The Significance Test Analysis of WUE Variation Trend

In this paper, the Mann–Kendall significance test was performed to test the significance of the WUE interannual rate of change in order to obtain the trend of significance change in WUE in the YRB from 1982 to 2018 (Figure 4 and Table 2). It was revealed that there was spatial heterogeneity in the trend of WUE changes in the YRB from 1982 to 2018, with a significant decrease (14.64%, Slope < 0, $p < 0.05$) of WUE in the southern and southeastern regions and a significant increase (47.07%, Slope > 0, $p < 0.05$) in some regions of the upstream and midstream. The areas with a significant increase in WUE were mainly distributed in Gansu and northern Shaanxi, while the areas with a significant decrease in WUE are primarily located in southeastern Shanxi, southern Shaanxi, Henan, and Shandong. Considerable variations were detected in the geographical patterns of WUE trends during the periods 1982–2000 and 2000–2018. The WUE exhibited a significant downward trend (Slope < 0, $p < 0.05$) in the midstream and downstream of the YRB, mainly in the southern and southeastern parts of the YRB from 1982 to 2000. However, the WUE exhibited a significant upward trend from 2000 to 2018 in most regions (Slope > 0, $p < 0.05$), mainly including Gansu, Ningxia Hui Region, northern Shaanxi, northern Shanxi, and most of southern Inner Mongolia.

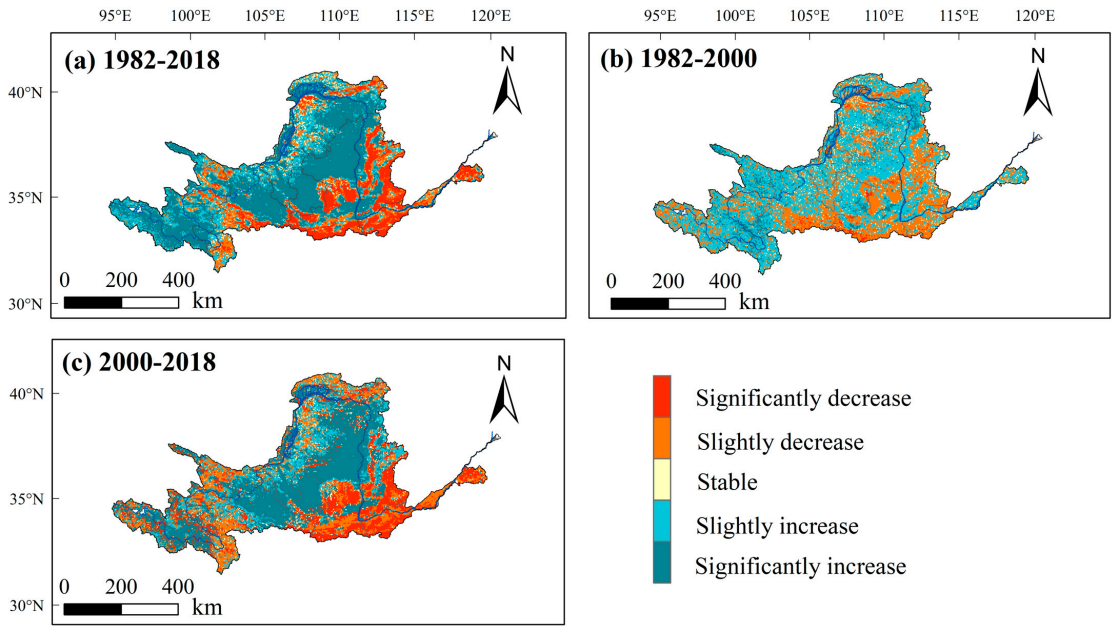

Figure 4. Spatial characteristics of significant variation trend of the WUE in different time periods.

Table 2. The percentage of area with significant variation trend of WUE.

Slope	Z_c	WUE Trend	Different Periods of Time		
			1982–2018	1982–2000	2000–2018
≥0.0005	≥1.96	Significantly increase	47.07	8.23	45.35
≥0.0005	−1.96–1.96	Slightly increase	21.03	55.35	16.92
–0.0005–0.0005	−1.96–1.96	Stable	4.32	4.78	4.11
<−0.0005	−1.96–1.96	Slightly decrease	12.94	29.82	15.05
<−0.0005	≤–1.96	Significantly decrease	14.64	1.82	18.57

Note: Slope (–0.0005, 0.0005) and Z_c (–1.96, 1.96) were defined as stable.

3.2. The WUE of Different LUCC

3.2.1. WUE of Different LUCC

We have analyzed the changes in WUE of different LUCC in the YRB during different periods (Figure 5). The results found that the WUE of different LUCC from 1982 to 2018 were forest (1.267 $gC \cdot kg^{-1} \cdot H_2O$), cropland (0.972 $gC \cdot kg^{-1} \cdot H_2O$), grassland (0.805 $gC \cdot kg^{-1} \cdot H_2O$), urban construction land (0.807 $gC \cdot kg^{-1} \cdot H_2O$) and other (0.654 $gC \cdot kg^{-1} \cdot H_2O$), respectively. WUE was highest in forest and grassland under different vegetation types. The forest WUE was 1.270 $gC \cdot kg^{-1} \cdot H_2O$ and 1.352 $gC \cdot kg^{-1} \cdot H_2O$ in 1982–2000 and 2000–2018, respectively. Forest WUE increased by 0.082 $gC \cdot kg^{-1} \cdot H_2O$ after 2000. Compared to the period from 1982 to 2000, the WUE of grasslands and croplands increased between 2000 and 2018. Specifically, the WUE of croplands improved by 0.144 $gC \cdot kg^{-1} \cdot H_2O$, while the WUE of grassland increased by 0.106 $gC \cdot kg^{-1} \cdot H_2O$. However, there has been a decrease in the WUE of urban areas, barren land, and water.

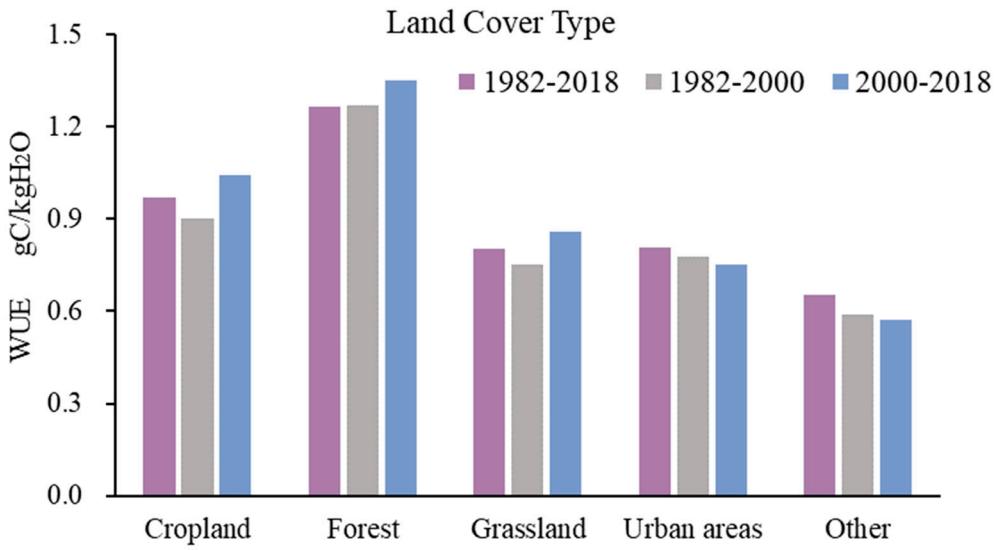

Figure 5. Variation in WUE in different land cover types.

3.2.2. Variations in WUE in Different Ecosystems

The WUE of different ecosystem types revealed a gradual upward trend from 1982 to 2018 in the YRB (Figure 6). The WUE of forest ecosystems showed a slowly increasing trend from 1982 to 2000, while it exhibited a significant upward trend starting from 2000 to 2018 at the rate of 0.79×10^{-2} $gC \cdot kg^{-1} \cdot H_2O \cdot a^{-1}$ (R^2 = 0.548). The WUE of farmland ecosystems in 1982–2000 and 2000–2018 showed an increasing trend at rates of 0.63×10^{-2} $gC \cdot kg^{-1} \cdot H_2O \cdot a^{-1}$ (R^2 = 0.237) and 0.55×10^{-2} $gC \cdot kg^{-1} \cdot H_2O \cdot a^{-1}$ (R^2 = 0.242), respectively.

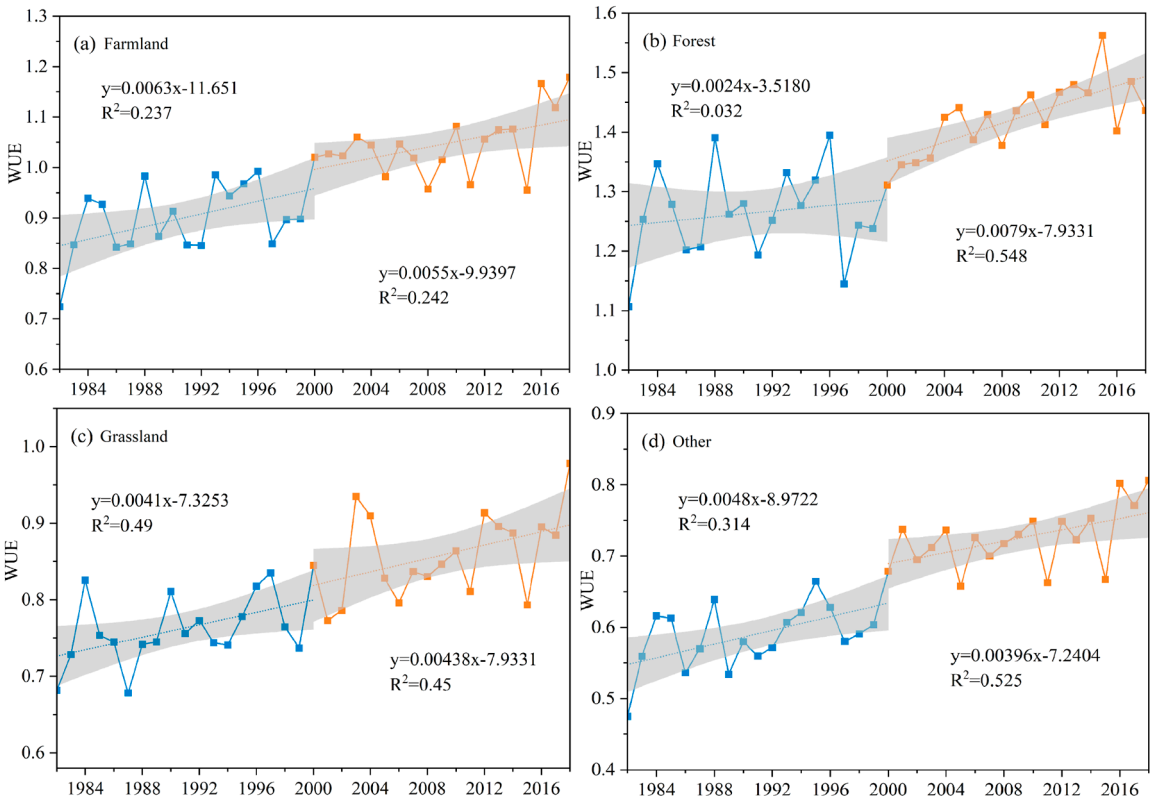

Figure 6. The trends of WUE for different ecosystem types in the YRB. (**a**) Farmland; (**b**) Forest; (**c**) Grassland; (**d**) Other.

The interannual rates of WUE in grassland ecosystems were 0.41 × 10^{-2} gC·kg^{-1}·H_2O·a^{-1} (R^2 = 0.49) and 0.44 × 10^{-2} gC·kg^{-1}·H_2O·a^{-1} (R^2 = 0.45) for 1982–2000 and 2000–2018, respectively. There are interannual differences in WUE between different ecosystem types, with forest ecosystems showing higher WUE than farmland, grassland, and other ecosystems. Moreover, the rate of increase in WUE of forest ecosystems from 2000 to 2018 was higher than other types.

3.3. WUE Dynamics Response to Climatic Variations

The partial correlation analysis method was applied to quantify the response of ecosystem WUE in the YRB to the main influencing factors from 1982 to 2018 (Figures 7 and 8). The WUE was positively correlated (R > 0) with temperature, precipitation, vapor pressure deficit (VPD), and SM by 58.27%, 79.08%, 47.70%, and 66.47%, respectively, and negatively correlated by 41.73%, 20.92%, 52.30%, and 33.53%, respectively. The highest percentage of areas exhibited positive correlation between WUE and precipitation (79.08%, R > 0), which was followed by SM (66.47%, R > 0). The area of positive correlation between WUE and VPD was the lowest among the four main climatic factors (47.70%, R > 0).

From its spatial distribution and the results of the correlation coefficient between WUE and climate factors in the YRB from 1982 to 2018 (significance test $p < 0.05$) (Figure 8), it is learned that the areas where WUE exhibited a significant positive relationship with precipitation (37.98%, R > 0, $p < 0.05$) are primarily located in the central and eastern regions of the YRB. The WUE had a significant positive correlation with SM (10.30%, R > 0, $p < 0.05$), primarily in central Gansu, northern Shaanxi, and sections of Inner Mongolia. However, there was a significant negative correlation between WUE and temperature (6.82%, R < 0, $p < 0.05$) in the west of Shaanxi, Baotou City in northern Inner Mongolia, and Henan Province in the downstream of the YRB; these regions were also the regions that showed a significant decrease in WUE. This indicates that temperature may cause a

reduction in the WUE to some extent. The results revealed that precipitation (37.98%, R > 0, $p < 0.05$) and SM (10.30%, R > 0, $p < 0.05$) were the primary climatic factors affecting the WUE in the YRB.

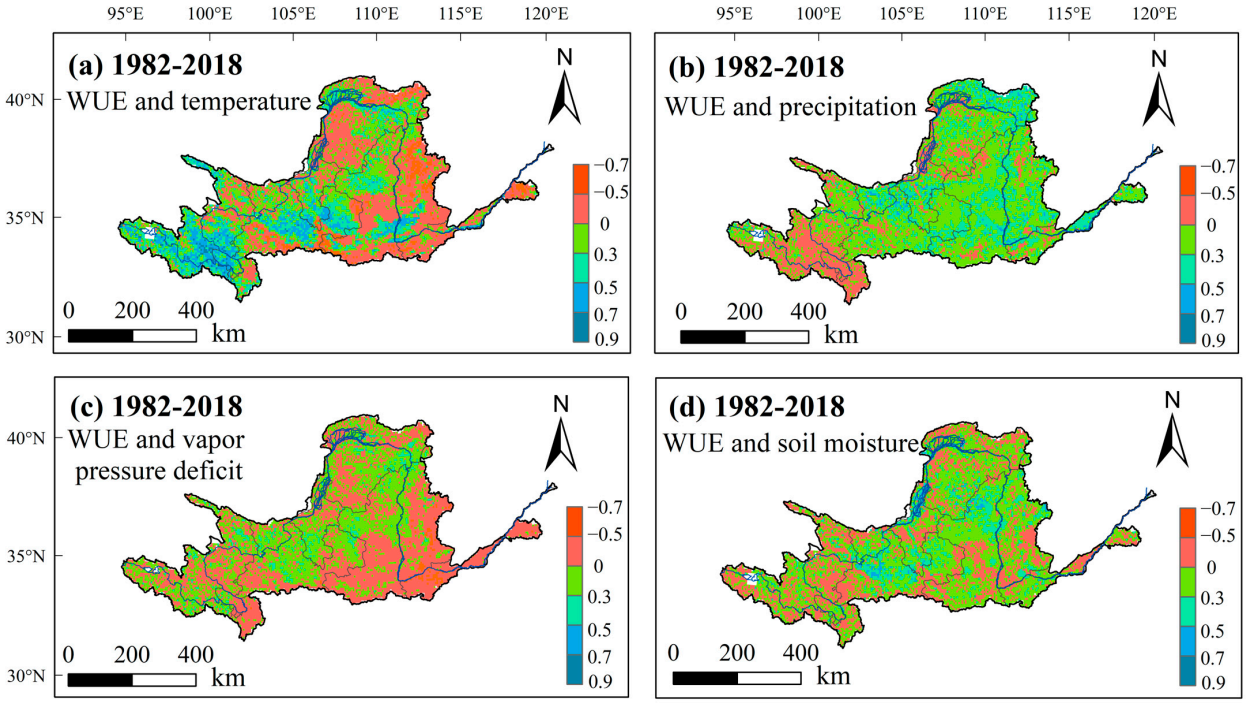

Figure 7. Spatial distribution of partial correlation coefficient between WUE and climate factors in the YRB from 1982 to 2018. (**a**) WUE and temperature; (**b**) WUE and precipitation; (**c**) WUE and vapor pressure deficit; (**d**) WUE and soil moisture.

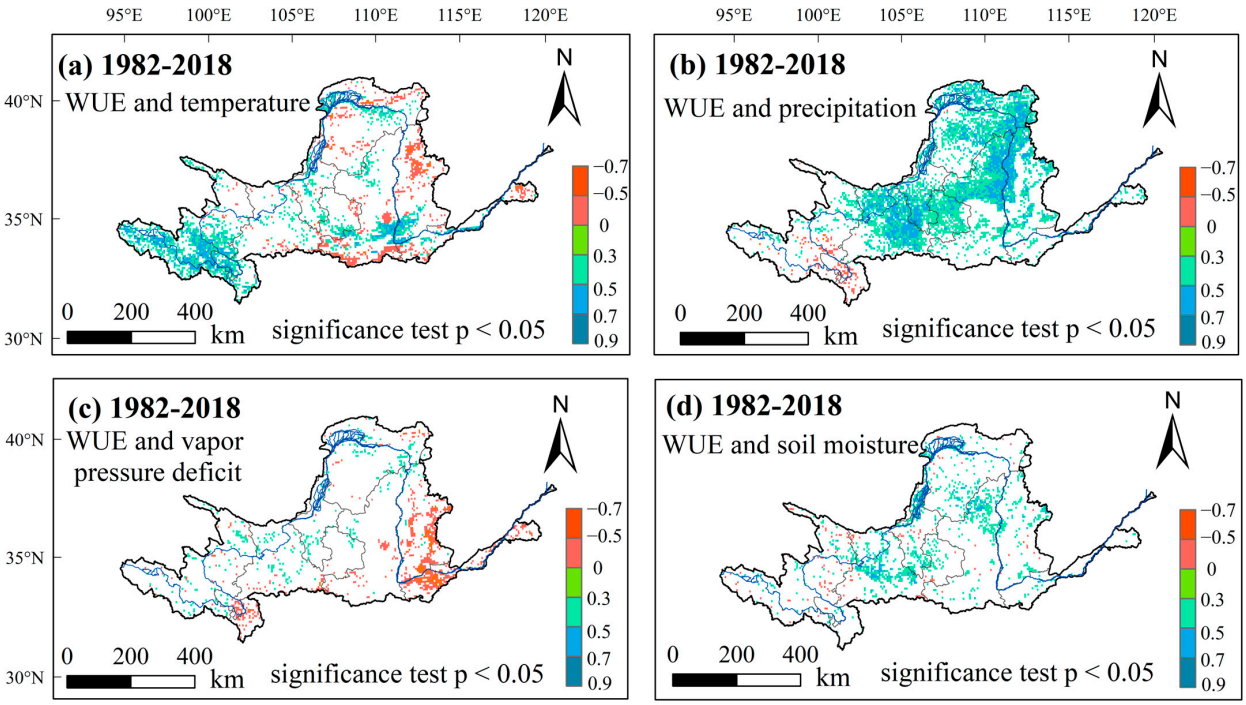

Figure 8. Spatial distribution of partial correlation coefficient between WUE and climate factors in the YRB from 1982 to 2018 (significance test $p < 0.05$). (**a**) WUE and temperature; (**b**) WUE and precipitation; (**c**) WUE and vapor pressure deficit; (**d**) WUE and soil moisture.

3.4. Response of WUE to GPP and ET

In order to explore the response of WUE changes to GPP and ET in the YRB from 1982 to 2018, this paper has categorized and discussed the effects of GPP and ET changes on WUE (Figure 9 and Table 3). The changes in WUE were divided into eight categories: WUE increase (GPP increase and ET increase; GPP increase and ET decrease; GPP decrease and ET increase; GPP decrease and ET decrease) and WUE decrease (GPP increase and ET increase; GPP increase and ET decrease; GPP decrease and ET increase; GPP decrease and ET decrease).

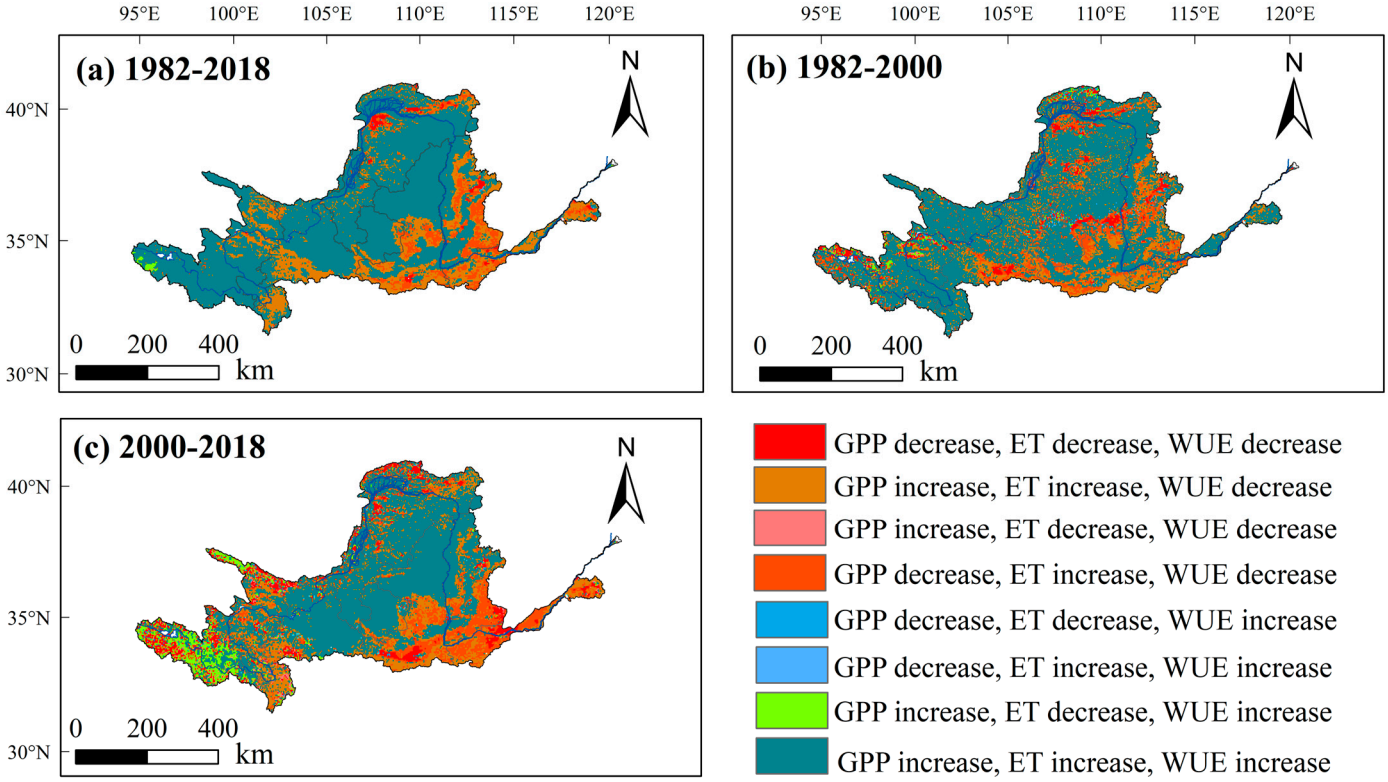

Figure 9. WUE changes in response to GPP and ET across different time periods.

Table 3. The percentage of area in response to changes in WUE to GPP and ET at different time periods.

WUE Change	GPP and ET Change	1982–2018		1982–2000		2000–2018	
		Area	Total	Area	Total	Area	Total
WUE decrease	GPP ↓ and ET ↓	1.10	29.61	7.35	39.76	3.51	34.07
	GPP ↓ and ET ↑	7.55		12.64		12.81	
	GPP ↑ and ET ↓	0.02		1.42		0.30	
	GPP ↑ and ET ↑	20.94		18.35		17.45	
WUE increase	GPP ↓ and ET ↓	0.03	70.39	0.67	60.24	0.37	65.93
	GPP ↓ and ET ↑	0.04		0.35		0.73	
	GPP ↑ and ET ↓	0.30		5.55		1.36	
	GPP ↑ and ET ↑	70.02		53.67		63.47	

Note: "↑" denotes an increase in the trend, "↓" denotes a decrease in the trend.

From 1982 to 2018, 70.39% of the WUE showed an increasing trend (Slope > 0), which was mainly attributable to GPP increase and ET increase, and the rate increase in GPP was higher than the rate increase in ET. The distribution is primarily in Inner Mongolia, southern Shaanxi, Ningxia, Gansu, and Qinghai. A total of 29.61% of WUE showed a decreasing trend (Slope < 0), mainly attributed to GPP increase and ET increase. However, the ET's increase rate was higher than that in GPP (20.94%), and there was a mismatch between the increase rates of ET and GPP. From 1982 to 2000, there were 60.24% of WUE,

which showed an increasing trend (Slope > 0), mainly attributed to GPP increase and ET increase (53.67%) and GPP increase and ET decrease (5.55%). However, 39.76% of the WUE exhibited a decrease trend, mainly because of the GPP decrease and ET increase (12.64%) and the GPP decrease and ET decrease (18.35%).

Figure 10 and Table 4 indicated the significant changes in GPP and ET on WUE after passing the test of significance (significance test $p < 0.05$). From 2000 to 2018, 65.39% of WUE showed an increasing trend (Slope > 0), mainly because of the GPP increase and ET increase, and the increase rate of GPP was greater than the increase rate of ET (63.47%). A total of 18.89% of WUE showed an increasing trend (Slope > 0, $p < 0.05$), and the significant increase in GPP and ET significantly contributed to the enhancement of WUE within the YRB. The part of the significant increase in WUE is mainly located in Gansu, Ningxia, and northern Shaanxi.

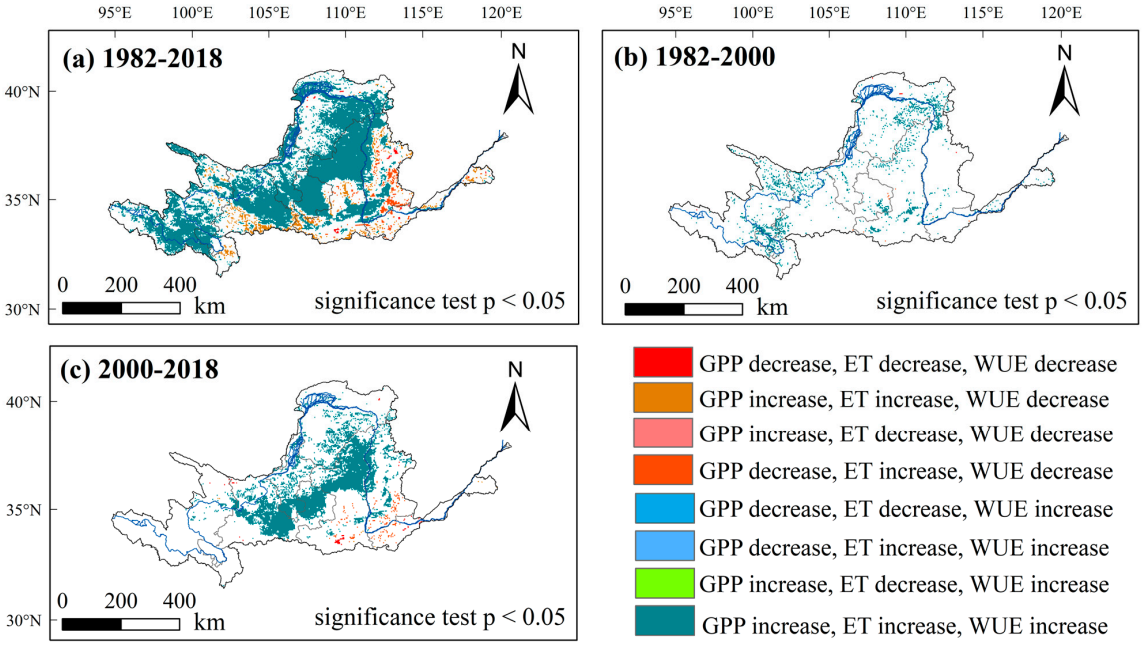

Figure 10. WUE significant changes in response to GPP significant changes and ET significant changes across different time periods (significant test $p < 0.05$).

Table 4. The percentage of area in response to the significant changes in WUE to GPP and ET at different time periods.

WUE Change	GPP and ET Change	1982–2018		1982–2000		2000–2018	
		Area	Total	Area	Total	Area	Total
WUE significant decrease	GPP ↓ and ET ↓	0.22	4.65	0.02	0.07	0.20	0.73
	GPP ↓ and ET ↑	1.42		0.04		0.50	
	GPP ↑ and ET ↓	/		/		/	
	GPP ↑ and ET ↑	3.01		/		0.04	
WUE significant increase	GPP ↓ and ET ↓	/	45.55	/	6.14	/	18.89
	GPP ↓ and ET ↑	/		/		/	
	GPP ↑ and ET ↓	/		/		/	
	GPP ↑ and ET ↑	45.55		6.14		18.89	

Note: "↑" represents a significant increase in the trend, "↓" represents a significant decrease in the trend. "/" indicates that the pixels has not passed the significance test.

4. Discussion

4.1. Dynamics and Drivers of WUE

This study employed linear regression analysis and the EEMD technique to explore the variations in WUE in the YRB from 1982 to 2018. The WUE exhibited a significant

upward trend (0.56×10^{-2} gC·kg^{-1}·H_2O·a^{-1}, $p < 0.05$) from 1982 to 2018 in the YRB. This trend was consistent with the findings of other scholars [8,9,17,30]. The area showing a significant increase in WUE (47.07%, Slope > 0, $p < 0.05$) was higher than the area with a significant decrease (14.64%, Slope < 0, $p < 0.05$). The spatial patterns of WUE changes in the YRB were significantly different between the periods of 1982–2000 and 2000–2018. It indicated that since the implementation of the policy of returning farmland to forest and grassland, the vegetation has increased to promote the increase of water use efficiency; the findings of this paper were consistent with those of other scholars [20,21,51–54].

This study evaluated the results of WUE outcomes across various plant communities, determining that forest WUE (1.267 gC·kg^{-1}·H_2O) was greater than that of cropland WUE (0.972 gC·kg^{-1}·H_2O), which in turn surpassed that of grassland WUE (0.805 gC·kg^{-1}·H_2O). From the analysis of different watersheds, it was learned that the WUE in the upstream (1.04 gC·kg^{-1}·H_2O) was higher than that in the downstream (0.95 gC·kg^{-1}·H_2O) and the midstream (0.81 gC·kg^{-1}·H_2O), which may be caused by the difference in vegetation structure between the upstream and midstream/downstream regions [5,23,30]. In the YRB, a sequential distribution pattern of grasslands, farmlands, and forests has emerged from the upstream to the midstream and downstream regions. Grasslands in the southwestern part of the basin and forests in the southeastern part demonstrate relatively high WUE due to higher GPP [20,21,40,55]. In contrast, the northern grassland ecosystems exhibit lower average annual precipitation and GPP. Consequently, more water is lost through soil evapotranspiration, resulting in comparatively lower WUE. This is primarily attributed to the "Returning Farmland to Forests and Grasslands" project [26,56–58], initiated in 2000, which expanded forest and grassland areas in the midstream region while decreasing farmland [6,33,54]. It has been observed that urbanization or town construction negatively impacts the WUE of vegetation, whereas ecological restoration initiatives can enhance the ecosystem's WUE in the YRB to some extent [7,59,60]. Therefore, we recommend implementing comprehensive water resource monitoring in the YRB to optimize the WUE of vegetation. This research offers crucial understanding for the efficient stewardship of water resources and environmental conservation within the area.

4.2. Sensitivity Analysis of WUE in the YRB

Global warming and other climatic factors have driven changes in WUE; WUE could diminish if ambient temperatures surpass the ideal range for botanical development. Moreover, elevated heat levels can accelerate the rate of water loss through transpiration, consequently amplifying the hydration requirements of vegetation [3,61–63]. Research has demonstrated that climate change modifies vegetation structure, thereby impacting the interplay between the carbon and hydrological cycles of ecosystems and consequently affecting WUE [61,64–66]. An et al. [4] demonstrated a decreasing trend in WUE in Xinjiang from 2000 to 2014 (Slope = −0.001), and determined that thermal conditions exerted a substantial influence on WUE, accounting for 87.7% of the variation. Tesfaye et al. [25] investigated WUE and its influencing factors in the Tekeze River region of northern Ethiopia from 1982 to 2014, identifying temperature and precipitation as key climatic factors affecting changes in Net Primary Productivity (NPP), ET, and WUE.

Traditional correlation analysis methods may not sufficiently account for the interrelationships among multiple variables [20,44,51]. In contrast, the partial correlation analysis method allows for the examination of the effects of multiple independent variables' effects on a dependent variable while considering their interactions and excluding the influence of other independent variables. This method enables a more accurate assessment of each variable's individual contribution to the dependent variable. The PCA method was utilized to assess the effects of temperature, precipitation, vapor pressure deficit, and soil moisture

on WUE. The findings revealed that the regions showing a positive and high correlation were 58.27%, 79.08%, 47.70%, and 66.47%, respectively, with the correlation between vapor pressure deficit and WUE being relatively lower. Precipitation and soil moisture are the primary climatic factors influencing the WUE of ecosystems in the YRB. Precipitation directly affects the availability of soil moisture, which in turn influences vegetation growth, water absorption, photosynthesis, and evapotranspiration processes [9,37,62,67]. Consequently, precipitation is closely linked to the WUE of vegetation [2,34,49]. The soil moisture affects the balance of photosynthesis and transpiration in plants [50,66,67], and when soil moisture becomes too low (e.g., drought conditions), the plant root system has difficulty in absorbing sufficient water [1,12,66–68]. This deficiency leads to reductions in photosynthesis and transpiration, stomatal closure, and ultimately a decline in WUE.

Meanwhile, the changes in ecosystem WUE were influenced by GPP and ET. Approximately 70.39% of the WUE in the YRB exhibited an increasing trend, primarily driven by increases in GPP and ET. WUE plays a regulatory role between GPP and ET. Under conditions of sufficient water supply, plants can increase GPP and WUE by increasing transpiration. However, under conditions of insufficient water supply, plants may reduce transpiration to maintain water, which may lead to a decrease in GPP, but WUE may increase due to a decrease in transpiration. The inconsistent rate of changes in GPP and ET could affect the change in WUE. Huang et al. [64] discovered that the increase in WUE was primarily driven by the rise in GPP, while ET exhibited no significant change under projected future warming scenarios. Amidst the context of global warming, the sequestration of carbon and the management of water resources have exhibited notable patterns. The disproportionate changes between GPP and ET highlight the important role of vegetation in the dynamics of the WUE ecosystem in the YRB. This research offers empirical evidence to facilitate the optimization of land management and water resource optimization.

4.3. Limitations

While this study has investigated WUE in the YRB, it is not without limitations. The data for GPP and ET used in this research were primarily derived from remote sensing observations or model simulations, and the accuracy of these data can be influenced by various factors [29,31,58]. Additionally, our analysis focused mainly on climatic factors affecting WUE, without comprehensively considering the impacts of hydrological conditions and land use changes [14,15,69]. Therefore, future research should delve deeper into the mechanisms by which climate change, land use change, and drought stress interact with WUE. It should also integrate multiple data sources and analytical tools to enhance the acquisition of high-precision data, optimize model parameterization, and improve validation methods, thereby advancing the understanding and prediction of ecosystem WUE.

5. Conclusions

This study analyzed the spatial-temporal variation characteristics of WUE and its influencing factors in the YRB and in different ecosystems from 1982 to 2018. The results show that: (1) From 1982 to 2018 the WUE exhibited a significant increase trend (0.56×10^{-2} $gC \cdot kg^{-1} \cdot H_2O \cdot a^{-1}$) in the YRB. The area showing a significant increase in WUE (47.07%, Slope > 0, $p < 0.05$) was higher than the area with a significant decrease (14.64%, Slope < 0, $p < 0.05$). The region of significant increase (Slope > 0, $p < 0.05$) in WUE in 2000–2018 (45.35%) was higher than that of 1982–2000 (8.23%), which was 37.12% higher in comparison. (2) Forest WUE (1.267 $gC \cdot kg^{-1} \cdot H_2O$) > Cropland WUE (0.972 $gC \cdot kg^{-1} \cdot H_2O$) > Grassland WUE (0.805 $gC \cdot kg^{-1} \cdot H_2O$) under different LUCC from 1982 to 2018. Forest had the highest WUE (1.267 $gC \cdot kg^{-1} \cdot H_2O$). The WUE of forest ecosystems (0.79×10^{-2} $gC \cdot kg^{-1} \cdot H_2O \cdot a^{-1}$) increased at a higher rate than that of farmland

(0.55×10^{-2} gC·kg^{-1}·H_2O·a^{-1}) and grassland (0.44×10^{-2} gC·kg^{-1}·H_2O·a^{-1}) from 2000 to 2018. (3) Precipitation (37.98%, $R > 0$, $p < 0.05$) and soil moisture (10.30%, $R > 0$, $p < 0.05$) are the main climatic factors affecting WUE in the YRB. A total of 45.55% of the WUE exhibited a significant increase trend (Slope > 0, $p < 0.05$), which is mainly attributed to the simultaneous increase in GPP and ET. This study provides important scientific support for water resource management and ecological protection in the Yellow River Basin.

Author Contributions: Conceptualization, J.Y., Y.W. and F.Q.; methodology, J.L. and X.Z.; data curation, J.L. and X.Z.; visualization, J.L. and M.Y.; writing—original draft, J.L. and S.C.; writing—review and editing, J.L., J.J. and L.W.; supervision, J.Y., Y.W. and F.Q. All authors have read and agreed to the published version of the manuscript.

Funding: This study was supported by The International Partnership Program of Chinese Academy of Sciences, grant number 177GJH2022020BS, The National Natural Science Foundation of China, grant number 32301564; The National Natural Science Foundation of China, grant number 42430514; The Science and Technology Projects in Guangzhou, grant number E33309.

Data Availability Statement: The original contributions presented in this study are included in the article. Further inquiries can be directed to the corresponding author.

Conflicts of Interest: The authors declare no conflicts of interest.

References

1. Cao, R.; Hu, Z.; Jiang, Z.; Yang, Y.; Zhao, W.; Wu, G.; Feng, X.; Chen, R.; Hao, G. Shifts in ecosystem water use efficiency on china's loess plateau caused by the interaction of climatic and biotic factors over 1985–2015. *Agric. For. Meteorol.* **2020**, *291*, 108100. [CrossRef]
2. Chang, X.; Wang, Z.; Wei, F.; Xiao, P.; Shen, Z.; Lv, X.; Shi, Y. Determining the Contributions of Vegetation and Climate Change to Ecosystem WUE Variation over the Last Two Decades on the Loess Plateau, China. *Forests* **2021**, *12*, 1442. [CrossRef]
3. Chen, Y.; Wang, Y.-P.; Huang, Y.; Tang, X.; Zhou, G.; Wang, C.; Chang, Z.; Yan, J. Temperature dependence of ecosystem carbon, nitrogen and phosphorus residence times differs between subtropical and temperate forests in China. *Agric. For. Meteorol.* **2022**, *326*, 109165. [CrossRef]
4. An, X. Responses of Water Use Efficiency to climate change in evapotranspiration and transpiration ecosystems. *Ecol. Indic.* **2022**, *141*, 109157. [CrossRef]
5. Cai, L.; Fan, D.; Wen, X.; Wang, H.; Badarifu; Wang, S. Spatiotemporal tendency of agricultural water use efficiency in the northernmost Yellow River: Indicator comparison and interactive driving factors. *J. Arid Environ.* **2022**, *205*, 104822. [CrossRef]
6. Du, Q.; Sun, Y.; Guan, Q.; Pan, N.; Wang, Q.; Ma, Y.; Li, H.; Liang, L. Vulnerability of grassland ecosystems to climate change in the Qilian Mountains, northwest China. *J. Hydrol.* **2022**, *612*, 128305. [CrossRef]
7. Jiao, F.; Xu, X.; Zhang, M.; Gong, H.; Liu, H.; Wang, K. Contributory factors of the secular trends to changes in ecosystem water-use efficiency in China. *J. Hydrol.* **2022**, *615*, 128690. [CrossRef]
8. Li, G.; Chen, W.; Li, R.; Zhang, X.; Liu, J. Assessing the spatiotemporal dynamics of ecosystem water use efficiency across China and the response to natural and human activities. *Ecol. Indic.* **2021**, *126*, 107680. [CrossRef]
9. Qin, G.; Meng, Z.; Fu, Y. Drought and water-use efficiency are dominant environmental factors affecting greenness in the Yellow River Basin, China. *Sci. Total Environ.* **2022**, *834*, 155479. [CrossRef] [PubMed]
10. Zheng, L.; Lu, J.; Chen, X. Drought offsets the vegetation greenness-induced gross primary productivity from 1982 to 2018 in China. *J. Hydrol.* **2024**, *632*, 130881. [CrossRef]
11. Deng, Y.; Wang, X.; Wang, K.; Ciais, P.; Tang, S.; Jin, L.; Li, L.; Piao, S. Responses of vegetation greenness and carbon cycle to extreme droughts in China. *Agric. For. Meteorol.* **2021**, *298–299*, 108307. [CrossRef]
12. Mu, Y.; Jia, X.; Ye, Z.; Guo, X.; Hao, S.; Zha, T.; Zhang, Y.; Han, C.; Gao, S.; Xing, F.; et al. Vegetation factors and atmospheric dryness regulate the dynamics of ecosystem water use efficiency in a temperate semiarid shrubland. *J. Hydrol.* **2024**, *639*, 131644. [CrossRef]
13. Yang, J.; Lu, X.; Liu, Z.; Tang, X.; Yu, Q.; Wang, Y. Atmospheric drought dominates changes in global water use efficiency. *Sci. Total Environ.* **2024**, *934*, 173084. [CrossRef]
14. Yue, P.; Zhang, Q.; Zhang, L.; Yang, Y.; Wei, W.; Yang, Z.; Li, H.; Wang, S.; Sun, X. Biometeorological effects on carbon dioxide and water-use efficiency within a semiarid grassland in the Chinese Loess Plateau. *J. Hydrol.* **2020**, *590*, 125520. [CrossRef]
15. Zhang, H.; Zhan, C.; Xia, J.; Yeh, P.J.F.; Ning, L.; Hu, S.; Wang, X.-S. The role of groundwater in the spatio-temporal variations of vegetation water use efficiency in the Ordos Plateau, China. *J. Hydrol.* **2022**, *605*, 127332. [CrossRef]

16. Zhang, T.; Peng, J.; Liang, W.; Yang, Y.; Liu, Y. Spatial-temporal patterns of water use efficiency and climate controls in China's Loess Plateau during 2000–2010. *Sci. Total Environ.* **2016**, *565*, 105–122. [CrossRef] [PubMed]
17. Li, D.; Wu, S.; Liu, L.; Zhang, Y.; Li, S. Vulnerability of the global terrestrial ecosystems to climate change. *Glob. Change Biol.* **2018**, *24*, 4095–4106. [CrossRef]
18. Wei, X.; He, W.; Zhou, Y.; Ju, W.; Xiao, J.; Li, X.; Liu, Y.; Xu, S.; Bi, W.; Zhang, X.; et al. Global assessment of lagged and cumulative effects of drought on grassland gross primary production. *Ecol. Indic.* **2022**, *136*, 108646. [CrossRef]
19. Yao, Y.; Liu, Y.; Fu, F.; Song, J.; Wang, Y.; Han, Y.; Wu, T.; Fu, B. Declined terrestrial ecosystem resilience. *Glob. Change Biol.* **2024**, *30*, e17291. [CrossRef]
20. Lamchin, M.; Lee, W.-K.; Jeon, S.W.; Wang, S.W.; Lim, C.H.; Song, C.; Sung, M. Long-term trend and correlation between vegetation greenness and climate variables in Asia based on satellite data. *Sci. Total Environ.* **2018**, *618*, 1089–1095. [CrossRef]
21. Lamchin, M.; Wang, S.W.; Lim, C.-H.; Ochir, A.; Pavel, U.; Gebru, B.M.; Choi, Y.; Jeon, S.W.; Lee, W.-K. Understanding global spatio-temporal trends and the relationship between vegetation greenness and climate factors by land cover during 1982–2014. *Glob. Ecol. Conserv.* **2020**, *24*, e01299. [CrossRef]
22. Chai, Y.; Miao, C.; Berghuijs, W.R.; Yang, Y.; Zhu, B.; Hu, Y.; Slater, L. Global reduction in sensitivity of vegetation water use efficiency to increasing CO_2. *J. Hydrol.* **2024**, *641*, 131844. [CrossRef]
23. Chen, F.; Yang, X.; Yu, Q.; Han, B. Quantifying the effects of diffuse photosynthetically active radiation on water use efficiency in different ecosystems. *Agric. For. Meteorol.* **2024**, *356*, 110191. [CrossRef]
24. Ji, R.; Wang, C.; Wang, P.; Wang, W.; Chen, N. Quantitative analysis of spatiotemporal disparity of urban water use efficiency and its driving factors in the Yangtze River Economic Belt, China. *J. Hydrol. Reg. Stud.* **2024**, *51*, 101647. [CrossRef]
25. Tesfaye, S.; Taye, G.; Birhane, E.; van der Zee, S.E.A.T.M. Spatiotemporal variability of ecosystem water use efficiency in northern Ethiopia during 1982–2014. *J. Hydrol.* **2021**, *603*, 126863. [CrossRef]
26. Xue, Y.; Liang, H.; Zhang, B.; He, C. Vegetation restoration dominated the variation of water use efficiency in China. *J. Hydrol.* **2022**, *612*, 128257. [CrossRef]
27. Ding, Y.; Zhang, L.; He, Y.; Cao, S.; Gusev, A.; Guo, Y.; Ran, L.; Wei, X.; Mikalai, F. Nonlinear effects of agricultural drought on vegetation productivity in the Yellow River Basin, China. *Sci. Total Environ.* **2024**, *948*, 174903. [CrossRef] [PubMed]
28. Zhang, T.; Quan, W.; Tian, J.; Li, J.; Feng, P. Spatial and temporal variations of ecosystem water use efficiency and its response to soil moisture drought in a water-limited watershed of northern China. *J. Environ. Manag.* **2024**, *355*, 120251. [CrossRef]
29. Yan, S.; Li, M.; Sun, T.; Liu, Q.; Liang, L.; Wang, X.; Li, C. The complex drought effects associated with the regulation of water-use efficiency in a temperate water-limited basin. *J. Hydrol. Reg. Stud.* **2021**, *36*, 100864. [CrossRef]
30. Liu, S.; Xue, L.; Xiao, Y.; Yang, M.; Liu, Y.; Han, Q.; Ma, J. Dynamic process of ecosystem water use efficiency and response to drought in the Yellow River Basin, China. *Sci. Total Environ.* **2024**, *934*, 173339. [CrossRef] [PubMed]
31. Lu, C.; Ji, W.; Hou, M.; Ma, T.; Mao, J. Evaluation of efficiency and resilience of agricultural water resources system in the Yellow River Basin, China. *Agric. Water Manag.* **2022**, *266*, 107605. [CrossRef]
32. Chen, C.; Park, T.; Wang, X.; Piao, S.; Xu, B.; Chaturvedi, R.K.; Fuchs, R.; Brovkin, V.; Ciais, P.; Fensholt, R.; et al. China and India lead in greening of the world through land-use management. *Nat. Sustain.* **2019**, *2*, 122–129. [CrossRef]
33. Feng, Z.; Yang, Y.; Zhang, Y.; Zhang, P.; Li, Y. "Grain for Green" Policy and Its Impacts on Grain Supply in West China. *Land Use Policy* **2005**, *22*, 301–312. [CrossRef]
34. Li, J.; Xi, M.; Wang, L.; Li, N.; Wang, H.; Qin, F. Vegetation Responses to Climate Change and Anthropogenic Activity in China, 1982 to 2018. *Int. J. Environ. Res. Public Health* **2022**, *19*, 7391. [CrossRef]
35. Zhang, L.; Deng, C.; Kang, R.; Yin, H.; Xu, T.; Kaufmann, H.J. Assessing the responses of ecosystem patterns, structures and functions to drought under climate change in the Yellow River Basin, China. *Sci. Total Environ.* **2024**, *929*, 172603. [CrossRef] [PubMed]
36. Tian, F.; Zhu, Z.; Cao, S.; Zhao, W.; Li, M.; Wu, J. Satellite-observed increasing coupling between vegetation productivity and greenness in the semiarid Loess Plateau of China is not captured by process-based models. *Sci. Total Environ.* **2024**, *906*, 167664. [CrossRef] [PubMed]
37. Piao, S.; Wang, X.; Park, T.; Chen, C.; Lian, X.; He, Y.; Bjerke, J.W.; Chen, A.; Ciais, P.; Tømmervik, H.; et al. Characteristics, drivers and feedbacks of global greening. *Nat. Rev. Earth Environ.* **2019**, *1*, 14–27. [CrossRef]
38. Xin, Y.; Yang, Y.; Chen, X.; Yue, X.; Liu, Y.; Yin, C. Evaluation of IMERG and ERA5 precipitation products over the Mongolian Plateau. *Sci. Rep.* **2022**, *12*, 21776. [CrossRef]
39. Li, Y.; Xie, Z.X.; Qin, Y.C.; Zheng, Z.C. Estimating Relations of Vegetation, Climate Change, and Human Activity: A Case Study in the 400 mm Annual Precipitation Fluctuation Zone, China. *Remote Sens.* **2019**, *11*, 1159. [CrossRef]
40. Liu, H.; Li, X.J.; Mao, F.J.; Zhang, M.; Zhu, D.; He, S.B.; Huang, Z.H.; Du, H.Q. Spatiotemporal Evolution of Fractional Vegetation Cover and Its Response to Climate Change Based on MODIS Data in the Subtropical Region of China. *Remote Sens.* **2021**, *13*, 913. [CrossRef]

41. Liu, Y.; Li, Y.; Li, S.C.; Motesharrei, S. Spatial and Temporal Patterns of Global NDVI Trends: Correlations with Climate and Human Factors. *Remote Sens.* **2015**, *7*, 13233–13250. [CrossRef]
42. Liu, Y.Y.; Ren, H.Y.; Zheng, C.; Zhou, R.L.; Hu, T.M.; Yang, P.Z.; Zhang, W.; Wang, Z.Q.; Li, Y.; Zhang, Z.Y.; et al. Untangling the effects of management measures, climate and land use cover change on grassland dynamics in the Qinghai-Tibet Plateau, China. *Land Degrad. Dev.* **2021**, *32*, 4974–4987. [CrossRef]
43. Pang, G.; Wang, X.; Yang, M. Using the NDVI to identify variations in, and responses of, vegetation to climate change on the Tibetan Plateau from 1982 to 2012. *Quat. Int.* **2017**, *444*, 87–96. [CrossRef]
44. Hawinkel, P.; Swinnen, E.; Lhermitte, S.; Verbist, B.; Van Orshoven, J.; Muys, B. A time series processing tool to extract climate-driven interannual vegetation dynamics using Ensemble Empirical Mode Decomposition (EEMD). *Remote Sens. Environ.* **2015**, *169*, 375–389. [CrossRef]
45. Liu, H.; Jia, J.; Lin, Z.; Wang, Z.; Gong, H. Relationship between net primary production and climate change in different vegetation zones based on EEMD detrending—A case study of Northwest China. *Ecol. Indic.* **2021**, *122*, 107276. [CrossRef]
46. Chu, H.S.; Venevsky, S.; Wu, C.; Wang, M.H. NDVI-based vegetation dynamics and its response to climate changes at Amur-Heilongjiang River Basin from 1982 to 2015. *Sci. Total Environ.* **2019**, *650*, 2051–2062. [CrossRef]
47. Jiapaer, G.; Liang, S.L.; Yi, Q.X.; Liu, J.P. Vegetation dynamics and responses to recent climate change in Xinjiang using leaf area index as an indicator. *Ecol. Indic.* **2015**, *58*, 64–76. [CrossRef]
48. Li, J.; Xi, M.; Pan, Z.; Liu, Z.; He, Z.; Qin, F. Response of NDVI and SIF to Meteorological Drought in the Yellow River Basin from 2001 to 2020. *Water* **2022**, *14*, 2978. [CrossRef]
49. Li, H.; Zhang, H.Y.; Li, Q.X.; Zhao, J.J.; Guo, X.Y.; Ying, H.; Deng, G.R.; Wu, R.H.; Wang, S.L. Vegetation Productivity Dynamics in Response to Climate Change and Human Activities under Different Topography and Land Cover in Northeast China. *Remote Sens.* **2021**, *13*, 975. [CrossRef]
50. Li, Y.; Xie, Z.X.; Qin, Y.C.; Sun, Y.Y. Temporal-Spatial Variation Characteristics of Soil Erosion in the Pisha Sandstone Area, Loess Plateau, China. *Pol. J. Environ. Stud.* **2019**, *28*, 2205–2214. [CrossRef] [PubMed]
51. Eckert, S.; Hüsler, F.; Liniger, H.; Hodel, E. Trend analysis of MODIS NDVI time series for detecting land degradation and regeneration in Mongolia. *J. Arid Environ.* **2015**, *113*, 16–28. [CrossRef]
52. Nemani, R.R.; Keeling, C.D.; Hashimoto, H.; Jolly, W.M.; Piper, S.C.; Tucker, C.J.; Myneni, R.B.; Running, S.W. Climate-Driven Increases in Global Terrestrial Net Primary Production from 1982 to 1999. *Science* **2003**, *300*, 1560–1563. [CrossRef]
53. Wang, X.; Piao, S.; Ciais, P.; Li, J.; Friedlingstein, P.; Koven, C.; Chen, A. Spring temperature change and its implication in the change of vegetation growth in North America from 1982 to 2006. *Proc. Natl. Acad. Sci. USA* **2011**, *108*, 1240–1245. [CrossRef]
54. Zhu, Z.; Piao, S.; Myneni, R.B.; Huang, M.; Zeng, Z.; Canadell, J.G.; Ciais, P.; Sitch, S.; Friedlingstein, P.; Arneth, A.; et al. Greening of the Earth and its drivers. *Nat. Clim. Change* **2016**, *6*, 791–795. [CrossRef]
55. Ji, X.; Sun, Y.; Guo, W.; Zhao, C.; Li, K. Land use and habitat quality change in the Yellow River Basin: A perspective with different CMIP6-based scenarios and multiple scales. *J. Environ. Manag.* **2023**, *345*, 118729. [CrossRef]
56. Wu, X.; Zhao, N.; Wang, Y.; Zhang, L.; Wang, W.; Liu, Y. Cropland non-agriculturalization caused by the expansion of built-up areas in China during 1990–2020. *Land Use Policy* **2024**, *146*, 107312. [CrossRef]
57. Xu, D.; Wang, Z. Identifying land restoration regions and their driving mechanisms in inner Mongolia, China from 1981 to 2010. *J. Arid Environ.* **2019**, *167*, 79–86. [CrossRef]
58. Zhuang, J.; Li, Y.; Bai, P.; Chen, L.; Guo, X.; Xing, Y.; Feng, A.; Yu, W.; Huang, M. Changed evapotranspiration and its components induced by greening vegetation in the Three Rivers Source of the Tibetan Plateau. *J. Hydrol.* **2024**, *633*, 130970. [CrossRef]
59. Deng, X.; Zhang, L. Spatio-temporal disparity of water use efficiency and its influencing factors in energy production in China. *Ecol. Inform.* **2022**, *71*, 101779. [CrossRef]
60. Dong, G.; Zhao, F.; Chen, J.; Qu, L.; Jiang, S.; Chen, J.; Shao, C. Divergent forcing of water use efficiency from aridity in two meadows of the Mongolian Plateau. *J. Hydrol.* **2021**, *593*, 125799. [CrossRef]
61. Chen, Z.; Wang, W.; Cescatti, A.; Forzieri, G. Climate-driven vegetation greening further reduces water availability in drylands. *Glob. Change Biol.* **2022**, *29*, 1628–1647. [CrossRef] [PubMed]
62. Li, Y.; Qin, Y.; Rong, P. Evolution of potential evapotranspiration and its sensitivity to climate change based on the Thornthwaite, Hargreaves, and Penman–Monteith equation in environmental sensitive areas of China. *Atmos. Res.* **2022**, *273*, 106178. [CrossRef]
63. Luo, W.; Muraina, T.O.; Griffin-Nolan, R.J.; Ma, W.; Song, L.; Fu, W.; Yu, Q.; Knapp, A.K.; Wang, Z.; Han, X.; et al. Responses of a semiarid grassland to recurrent drought are linked to community functional composition. *Ecology* **2023**, *104*, e3920. [CrossRef]
64. Huang, M.-T.; Zhai, P.-M. Impact of extreme seasonal drought on ecosystem carbon–water coupling across China. *Adv. Clim. Chang. Res.* **2024**, *15*, 914–923. [CrossRef]
65. Li, T.; Xia, J.; Zhang, L.; She, D.; Wang, G.; Cheng, L. An improved complementary relationship for estimating evapotranspiration attributed to climate change and revegetation in the Loess Plateau, China. *J. Hydrol.* **2021**, *592*, 125516. [CrossRef]

66. Li, X.; Zha, T.; Liu, P.; Bourque, C.P.A.; Jia, X.; Tian, Y.; Jin, C.; Wei, X.; Liu, X.; Zhao, H.; et al. Interannual variation in gross ecosystem production and evapotranspiration in a temperate semiarid grassland undergoing vegetation recovery. *Agric. For. Meteorol.* **2023**, *341*, 109672. [CrossRef]
67. Li, W.; Migliavacca, M.; Forkel, M.; Denissen, J.M.C.; Reichstein, M.; Yang, H.; Duveiller, G.; Weber, U.; Orth, R. Widespread increasing vegetation sensitivity to soil moisture. *Nat. Commun.* **2022**, *13*, 3959. [CrossRef]
68. McDowell, N.G.; Coops, N.C.; Beck, P.S.; Chambers, J.Q.; Gangodagamage, C.; Hicke, J.A.; Huang, C.Y.; Kennedy, R.; Krofcheck, D.J.; Litvak, M.; et al. Global satellite monitoring of climate-induced vegetation disturbances. *Trends Plant Sci.* **2015**, *20*, 114–123. [CrossRef] [PubMed]
69. Yang, X.; Tian, S.; You, W.; Jiang, Z. Reconstruction of continuous GRACE/GRACE-FO terrestrial water storage anomalies based on time series decomposition. *J. Hydrol.* **2021**, *603*, 127018. [CrossRef]

Disclaimer/Publisher's Note: The statements, opinions and data contained in all publications are solely those of the individual author(s) and contributor(s) and not of MDPI and/or the editor(s). MDPI and/or the editor(s) disclaim responsibility for any injury to people or property resulting from any ideas, methods, instructions or products referred to in the content.